Dual-focus fluorescence correlation spectroscopy: a robust tool for studying molecular crowding

Claus B. Müller,[a] Thomas Eckert,[a] Anastasia Loman,[b] Jörg Enderlein*[b] and Walter Richtering*[a]

Received 17th July 2008, Accepted 11th December 2008
First published as an Advance Article on the web 9th February 2009
DOI: 10.1039/b812289j

Conventional single-focus fluorescence correlation spectroscopy (FCS) is often used for studying molecular diffusion in crowded environments. However, these measurements usually deal with concentrations of the crowding agent far beyond the overlap-concentration, resulting in a crowding effect which slows down the diffusion coefficient by several orders of magnitude. In the present paper, we would like to study the transition range from free diffusion to crowding. Therefore, high accuracy of the determination of the diffusion coefficient is needed. In the majority of cases, the local refractive index in a sample is different from the refractive index of the immersion medium of the used objective. To achieve a high accuracy during experiments it is necessary to account for the refractive index mismatch in single-focus FCS calculations. In this work, we study theoretically and experimentally the influence of the refractive index mismatch on performance of single-focus FCS as well as the recently developed dual-focus FCS (2fFCS). By looking at the transition from free tracer diffusion to crowding it is shown that, in contrast to conventional FCS, 2fFCS allows measuring absolute values of the diffusion coefficient and its change in the range of half an order of magnitude. Even under conditions of strong refractive index mismatch between sample and immersion medium, without the need of additional calibration. This is demonstrated on a system of fluorescently labeled 70 kDa dextrane in an unlabeled 70 kDa dextrane matrix. Therefore, 2fFCS is a perfect tool for investigating molecular dynamics in crowded environments.

1 Introduction

Transport effects and hindered diffusion are important in many applications including rheology, colloid and polymer science,[1,2] and biological and biochemical processes.[3,4] Crowded environments consisting of highly concentrated solutions of macromolecules have a large impact on reaction rates,[5,6] equilibrium constants, or self-assembly of super-molecular structures.[7] It also induces depletion interactions, causing macromolecules to segregate according to their size due to the increase in free volume accessible to solutes.[8]

Fluorescence correlation spectroscopy (FCS) is a powerful tool for investigating the diffusion of fluorescently tagged molecules in crowded environments. So far, many FCS studies have been carried out on protein–protein solutions,[9–11] protein–dextrane solutions[10,12] or other combinations with dextrane,[13,14] because molecular crowding is supposed to play an important role in physiological systems.

Other publications[10,13,15] describe single-focus FCS experiments, which deal with high concentrations of crowding agent, resulting in a strong influence (several orders of magnitude) on the diffusion coefficient, or attempt to study diffusion of polymer chains with high accuracy.[4] However, if the observed range of concentration is the transition range from free to hindered diffusion, where the diffusion coefficient decreases by half an order of magnitude, single-focus FCS reaches its limits.

An important factor for FCS inaccuracy is usually the strong refractive index mismatch between the sample and the immersion medium of the used objective, necessitating extensive calibration for conventional FCS prior to each measurement.[14,16,17]

This becomes time consuming when measuring tracer diffusion in different samples with varying amount of crowding agent and thus varying refractive index of the sample. Although FCS calibration might be an acceptable way of taking into account these refractive index changes, it still requires lengthy calibration measurements for each sample concentration.

Even then, it is still difficult to obtain precise absolute values for a diffusion coefficient. The main reason is the dependence of size and shape of the detection volume (described by the molecule detection function or MDF) on excitation intensity due to optical saturation effects, see *e.g.* ref. 18 and 19. Another reason, due to refractive index mismatch, is that the MDF becomes increasingly sensitive to the absolute position of the focus above the cover-slide surface.[19,20] Thus, as either the intensity (or optical saturation properties of the used dye) or focus position or both do change between two measurements, they cannot be compared or calibrated against each other, which makes determining correct absolute values of diffusion coefficients rather difficult.

In ref. 18 and 19, we presented theoretical estimates of the influence of refractive index mismatch on the outcome of conventional single-focus FCS experiments. Here, we will study this topic in more detail, comparing theoretical and experimental measurements for both single-focus as well as dual-focus FCS. We

[a]*Institute of Physical Chemistry, RWTH Aachen University, 52056 Aachen, Germany. E-mail: richtering@rwth-aachen.de*
[b]*III. Institute of Physics, Georg August University, 37077 Göttingen, Germany. E-mail: joerg.enderlein@physik3.gwdg.de*

present extensive numerical calculations of the MDF as a function of refractive index and focus position, and its impact on the final autocorrelation function (ACF). The results allow the estimation of the systematic errors introduced in conventional single-focus FCS experiments due to refractive index mismatch.

As will be shown, the recently developed 2fFCS[18] allows these problems to be circumvented. The core idea of 2fFCS is to introduce an external length scale into the measurement which is not affected by refractive index related optical aberrations. This is done by creating two laterally shifted but overlapping foci with well known and fixed distances. By measuring the ACFs for each focus as well as the cross-correlation function (CCF) between the foci, and performing a global fit of all three curves, it is possible to determine absolute values of a diffusion coefficient without further calibration or referencing. The resulting accuracy and reproducibility of determined diffusion coefficients is superior to conventional single-focus FCS, making 2fFCS a very useful tool for investigating systems with inherently large optical aberrations as caused by *e.g.* refractive index mismatch.

The capability of 2fFCS is exemplary, demonstrated by measuring the self-diffusion of labelled dextrane in a concentrated solutions of 70 kDa dextrane near the transition from free to hindered diffusion. The measured data are evaluated with a conventional single-focus FCS model as well as with an extended 2fFCS model. As will be shown, the accuracy of 2fFCS is much higher than that of single-focus FCS, allowing direct measurements without further calibration. Furthermore, results obtained with 2fFCS and with conventional dynamic light scattering (DLS) are compared. It is verified that 2fFCS is able to provide values of tracer diffusion in contrast to DLS experiments, which show collective relaxation of the whole crowding environment.

2 Materials and instruments

2.1 Materials

The solvent LichroSolv water for chromatography (No. 115333), was purchased from Merck KGaA (Darmstadt, Germany). FITC fluorescein-iso-thiocyanate (FITC)-labeled dextrane was obtained from Fluka (70 kDa: No. 46945, FITC:Glucose = 1:250). Unlabeled dextrane 70 kDa No. A1847 was obtained from AppliChem (Darmstadt, Germany). The hydrodynamic radius was determined to be $R_h = 7.4 \pm 0.5$ nm.

2.2 Sample preparation

A stock solution of 3.5×10^{-7} g/l FITC-dextrane 70 kDa in LichroSolv water was prepared. Samples containing unlabeled 70 kDa dextranes were prepared by solving dried unlabeled dextrane powder in stock solution. Reported concentrations of composite solutions are always cumulative concentrations of labeled and unlabeled dextranes.

2.3 Instruments

Viscosity of dextrane solutions was determined with a Lauda PVS viscosity system, equipped with a micro Ubbelode capillary No. 1011219 and a temperature controlled water bath.

Dynamic light scattering (DLS) measurements were performed on a standard ALV 5000 system, equipped with a laser of 633 nm wavelength. Scattering intensity was detected at angles of 60°, 90°, and 120°, respectively, and the hydrodynamic radius was calculated with a second order cumulant fit using the Stokes–Einstein relation. The measurement system was equipped with a temperature controlled water bath giving a precision in sample temperature stabilization of $\pm$ 0.2 K.

2fFCS experiments were performed on a modified MicroTime200 (PicoQuant Berlin, Germany). Modification and calibration are described in detail in ref. 21 and 22. The setup was equipped with two identical, linearly polarized pulsed laser sources at 470 nm wavelength (LDH-P-C-470B, PicoQuant, Berlin, Germany). To discriminate backscattered excitation light from fluorescence, a major triple band dichroic z470/532/638rpc (AHF-Anaysentechnik, Tübingen, Germany), was inserted into the detection optical path. The temperature was controlled by a homemade temperature regulator.[23] The absolute accuracy of temperature in the confocal volume was $\pm$0.1 K with a precession of $\pm$0.05 K. The sample stayed in sealed sample cells to prevent solvent evaporation.[24] For longtime measurements, the microscope was equipped with an automatic immersion water supply.

3 Theory

3.1 Calculation of molecule detection function (MDF)

In FCS experiments a collimated Gaussian excitation laser beam is focused through a high N. A. microscope objective and the excited fluorescence is collected by the same objective (epi-fluorescence setup). Thus, the calculation of the molecule detection function proceeds in two steps: first the excitation intensity profile is calculated and second, the light collection efficiency function (CEF) is computed. For fast rotating molecules, where rotational diffusion is much faster than the fluorescence decay time, or for homogeneously labeled beads, the MDF is satisfactorily described by the product of the CEF with the excitation intensity profile.

The main difference between the MDF and the conventional point spread function (PSF) is that the MDF takes also into account optical saturation of a dye as well as a potential coupling between its excitation and emission dipole orientation, for a theoretical discussion see ref. 19 and also ref. 17. Although all of the effects discussed here for the MDF are equally applicable to the PSF as used in conventional imaging confocal microscopy, the latter is usually much less sensitive to small deformations of the PSF than FCS is.

Fluorescing molecules are assumed to be electric dipole absorbers and emitters. Following the fundamental work of Richards and Wolf,[25,26] the excitation intensity distribution $I_{ex}(r)$ is calculated by expanding the electric field in sample space into a superposition of plane waves. This plane wave representation is ideally suited to take into account aberrations introduced by planar layers of different refractive index between the front lens of the objective and the focal spot, as is the case of coverslide thickness deviations or refractive index mismatch between sample solution and objective's immersion medium. The computational details of such calculations are presented in several publications, see ref. 19 and 27–33.

To calculate the CEF, which is proportional to the probability distribution for detecting a fluorescence photon from a given position r, one calculates the Poynting energy flux[34] through the confocal

aperture as generated by a molecule at a given position and averages this energy flux over all the molecule's possible orientations. Details for these calculations can be found in ref. 19 and 35–38.

Under ideal, aberration-free conditions, the MDF $U(\vec{r})$ can be perfectly approximated by a modified Gauss–Lorentz profile as given by[18]

$$U(\vec{r}) = \frac{\kappa(z)}{w^2(z)} \exp\left[-\frac{2}{w^2(z)}\left(x^2 + y^2\right)\right] \quad (1)$$

where x, y, and z are Cartesian coordinates with the z-axis along the optical axis. Functions $w(z)$ and $\kappa(z)$ are given by

$$w(z) = w_0 \sqrt{1 + \left(\frac{\lambda_{ex} z}{\pi w_0^2 n}\right)^2} \quad (2)$$

and

$$\kappa(z) = 1 - \exp\left(-\frac{2a^2}{R_0^2 + (\lambda_{em} z/\pi R_0 n)^2}\right) \quad (3)$$

where λ_{ex} and λ_{em} are excitation and center emission wavelengths, n is the sample refractive index, a is the confocal pinhole radius.

The robustness of 2fFCS against the different optical peculiarities such as coverslide thickness, sample refractive index, or optical saturation was extensively studied in ref. 17 by exact modeling of 2fFCS experiments for a large range of different experimental parameters. It should be mentioned that deviation of the coverslide thickness from its design value as well as deviation of the sample refractive index from the value of the immersion medium introduce very similar optical aberrations. Robustness of 2fFCS against the latter was experimentally shown already in the original 2fFCS publication of ref. 18. Robustness of 2fFCS against optical saturation, the most disturbing problem in conventional FCS, was experimentally shown in ref. 39.

3.2 Single-focus ACF calculation

The calculation of ACF, $g(\tau)$, is equivalent to determining the probability of detecting a photon at time $t + \tau$ if there had been a photon detection event at time t. It was shown in detail in ref. 19, that the ACF can be calculated from the MDF as

$$\begin{aligned} g(\tau) = {} & \pi c \sum_{m=0}^{\infty} (1 + \delta_{m,0}) \\ & \int \mathrm{d}\rho\rho \int \mathrm{d}z U_m(\rho, z) F_m(\rho, z, \tau) \\ & + \left[2\pi c \int \mathrm{d}\rho\rho \int \mathrm{d}z U_0(\rho, z) + I_{bg} \right]^2 \end{aligned} \quad (4)$$

where the function F_m is given by

$$\begin{aligned} F_m(\rho, z, \tau) = {} & \frac{2\pi i^m exp(-\rho^2/4D\tau)}{(4\pi D\tau)^{3/2}} \\ & \int_0^{\infty} \mathrm{d}\rho_0 \rho_0 \int_{-\infty}^{\infty} \mathrm{d}z_0 U_m(\rho_0, z_0) J_m\left(\frac{i\rho\rho_0}{2D\tau}\right) \\ & \exp\left[-\frac{\rho_0^2 + (z - z_0)^2}{4D\tau}\right] \end{aligned} \quad (5)$$

and the following abbreviations have been used: D is the diffusion coefficient of the diffusing molecules, c is their concentration, $\delta_{m,n}$ is Kronecker's symbol being unity for $m = n$ and zero otherwise, and J_m denotes Bessel functions of the first kind. The integrations in the above equations have to be done numerically. Because the MDF falls off rapidly to zero when moving away from the focus center, the integrations converge rather quickly to a final value when numerically integrating over larger and larger values of ρ and z.

In the present contribution, we study the impact of focus position, excitation wavelength, and size of confocal aperture on an single-focus FCS measurement. Furthermore, we consider the influence of instrumental parameters such as objective magnification, diameter of excitation beam and focal length of the tube lens. This is done by calculating the ACF (eqn 4 + 5) from the wave-optically calculated MDF as explained above.

The apparent diffusion times τ, which we define as inflection point of the ACF, were determined by comparing the calculated ACFs at various refractive indices with the ideal ACF (with apparent diffusion time τ_0) under ideal optical conditions at $n_D = 1.333$ (see also ref. 20). This allows the calculation of the ratio of diffusion times, τ/τ_0, which is equal to the ratio D/D_0 of the diffusion coefficients.

3.3 Dual-focus FCS fitting

As we have shown in previous publications,[18–20] diffusion coefficients obtained from single-focus FCS show a strong dependency on refractive index mismatch. To overcome the pitfalls of single-focus FCS, we have developed the novel technique of dual-focus FCS (2fFCS). The core idea is to introduce an external length scale into a FCS measurement. Two laterally shifted but overlapping foci with well known and fixed distance are created as described in ref. 18. Although optical aberrations may distort the shape of the MDF of each focus, the center distance between them and thus the intrinsic ruler used for the diffusion coefficient calculation is not changed by these effects, in contrast to single-focus FCS, where the diffusion coefficient is referenced to the size and shape of the MDF.[40–43]

For obtaining an absolute value of a diffusion coefficient from a 2fFCS measurement, it is assumed that the MDF of each focus is well described by the model of eqn 1. Then the ACFs and CCF are given by the general expression

$$\begin{aligned} g(t) = {} & g_{\infty}(\delta) + 2\varepsilon_1\varepsilon_2 c \sqrt{\frac{\pi}{Dt}} \\ & \int_{-\infty}^{\infty} dz_1 \int_{-\infty}^{\infty} dz_2 \frac{\kappa(z_1)\kappa(z_2)}{8Dt + w^2(z_1) + w^2(z_2)} \\ & \exp\left[-\frac{(z_2 - z_1)^2}{4Dt} - \frac{2\delta^2}{8Dt + w^2(z_1) + w^2(z_2)}\right] \end{aligned} \quad (6)$$

which has to be evaluated numerically. Here, δ is the lateral distance between the foci, ε_1 and ε_2 are factors proportional to the overall excitation intensity and detection efficiency in each laser, c is the concentration of fluorescent molecules and D is the diffusion coefficient. To calculate the ACF of each focus, one has to set $\delta = 0$ and to replace $\varepsilon_1\varepsilon_2$ by either ε_1^2 or ε_2^2, respectively.

Fitting of experimental data is done simultaneously for ACFs, which are identical in shape, and CCF to have as fit parameters $\varepsilon_1\sqrt{c}$, $\varepsilon_2\sqrt{c}$ and D.

By measuring the ACF for each focus separately as well as the CCF of the fluorescence between both foci and fitting both the ACFs and CCF globally with model eqn 6 allows the extraction of absolute values of the diffusion coefficient without any further calibration. The hydrodynamic radius R_h is then calculated from the obtained diffusion coefficient by the well known Stokes–Einstein equation:

$$R_h = \frac{kT}{6\pi\eta D} \tag{7}$$

It is important to note that the model eqn 1 will not be, in general, an exact description of the real MDF, especially when large aberrations are present. But the resulting generic function eqn 6 for the ACF/CCF still yields accurate results for the diffusion coefficient, as was shown in several previous publications.[18–20,22]

4 Results and discussion

4.1 Influence of refractive index mismatch on single-focus FCS

In FCS measurements, a collimated laser beam is focused through an objective with high numerical aperture (NA = 1.2) into the sample solution. Focusing as well as detection will be optimal (aberration-free) only if the refractive index of the objective's immersion medium and that of the sample solution are equal. For water immersion objectives, perfect focusing and imaging is thus achieved only when measuring in pure water solutions with a refractive index of $n_D = 1.333$.

In experiments with refractive index mismatch, the apparent diffusion time is influenced by focus position. In Fig 1, we display iso-surfaces where the MDF has fallen off to $1/e$, $1/e^2$ and $1/e^3$ from its maximum value at the focus center, for various focus positions and sample refractive indices. Calculation parameters are λ_{ex} = 530 nm, λ_{em} = 570 nm, confocal aperture diameter 200 μm, 10 mm excitation beam diameter, 180 mm focal distance of tube lens, and 60× objective magnification.

The indicated position is the nominal focus position under aberration-free conditions, the additional shift as seen in the figures is caused by the refractive index mismatch. It is important to note, that the MDF strongly increases in size with higher refractive indices. For a focus position of 200 μm and $n_D = 1.450$, the MDF has a length of nearly 20 μm.

The variation of the refractive index between $n_D = 1.333$ and $n_D = 1.45$, covers the typical range of crowding agent concentrations and also the refractive index range of FCS measurements in most organic solvents. The apparent diffusion times are calculated by computing the time shift between the ACFs for different refractive indices and the ACF for $n_D = 1.333$. The black line refers to the same parameter set and is presented in each plot in Fig. 2 and 3 to compare variations of the presented parameters.

Another important parameter of the optical setup is the numerical aperture of the objective. In the practice of FCS, one always uses objectives with maximum possible aperture for maximizing the light collection efficiency of the setup. The effect of excitation laser beam radius, *i.e.* the effect of the effective aperture used in laser focusing, was extensively studied in ref. 17.

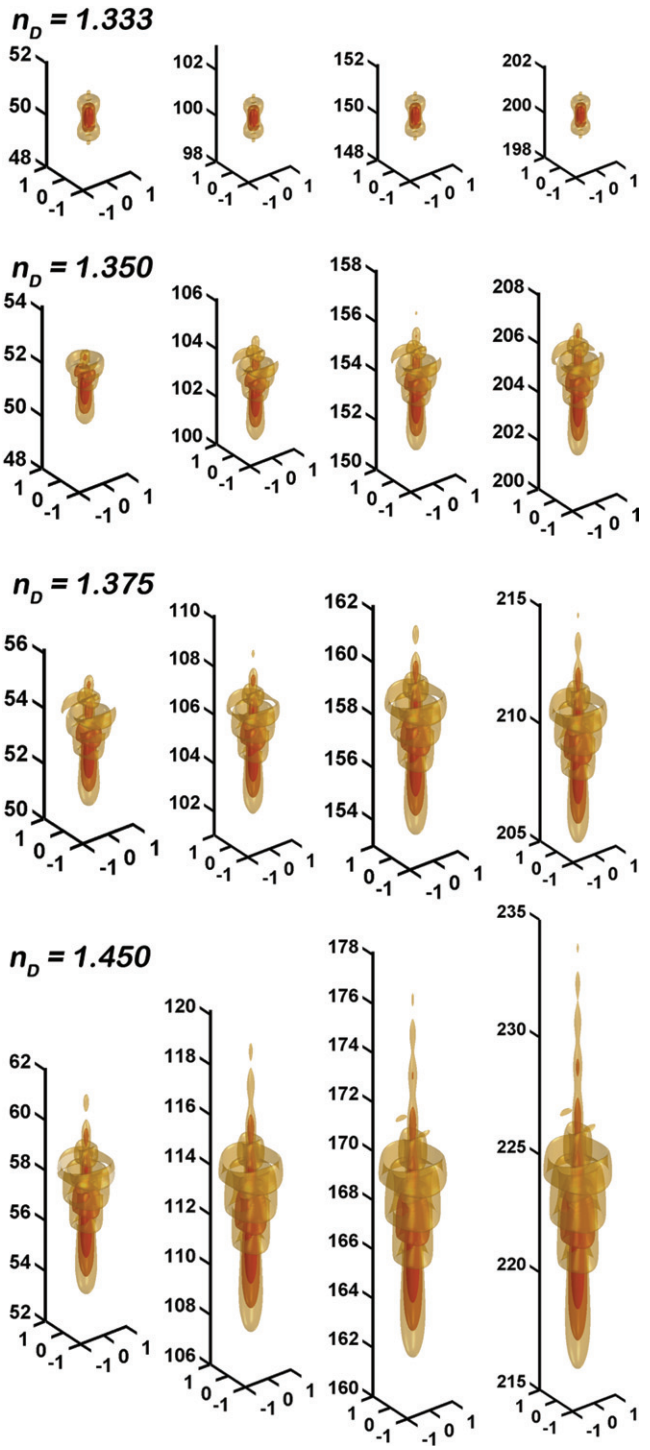

Fig. 1 Calculation of the molecule detection function for different focus positions (from left to right) at 50 μm, 100 μm, 150 μm and 200 μm and different refractive indexes (from top to bottom) at $n_D = 1.333$, $n_D = 1.350$, $n_D = 1.375$ and $n_D = 1.450$. Iso-surfaces are shown where MDF has fallen off to $1/e$, $1/e^2$ and $1/e^3$ of its maximum value at the focus center. All indicated numbers on axis are μm. The iso-surfaces are calculated for water immersion objective, corrected for immersion liquid with $n_D = 1.333$.

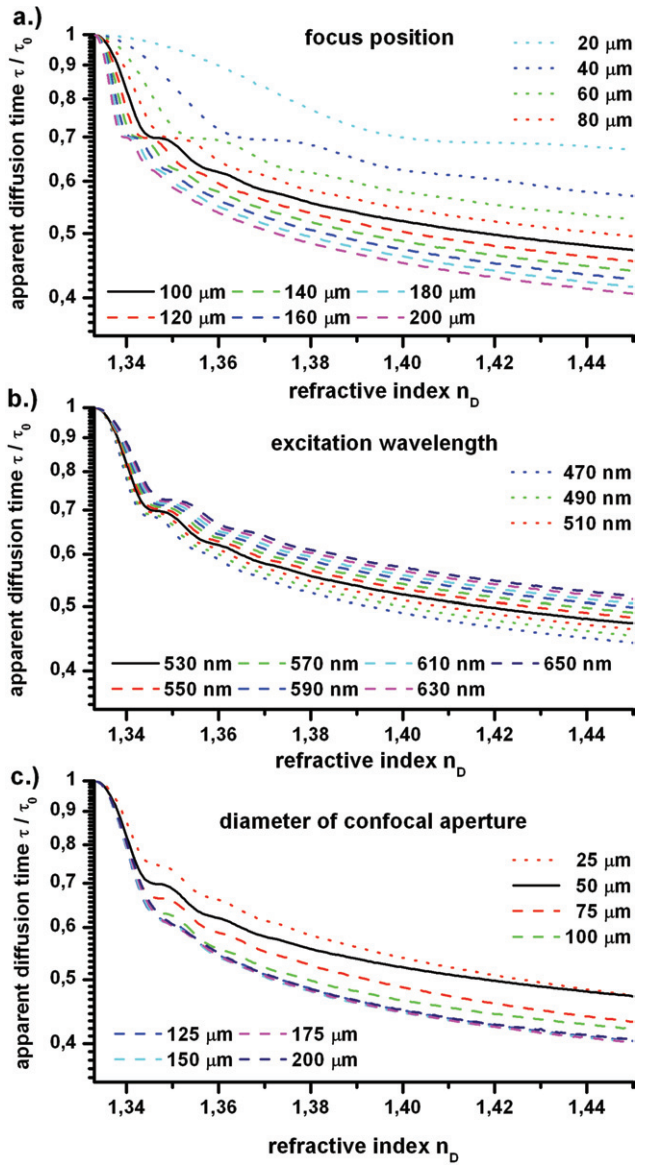

Fig. 2 Influence of experimental parameters [(a) focus position in the sample, (b) excitation wave length, (c) size of confocal aperture] due to the refractive index dependency of the apparent diffusion time. Simulation parameters if not indicated: focus position = 100 μm, λ_{ex} = 530 nm, $\lambda_{em} = \lambda_{ex}$ + 40 nm, confocal aperture = 50 μm, objective magnification = 60×, excitation beam diameter = 10 mm and tube lens focal distance = 180 mm.

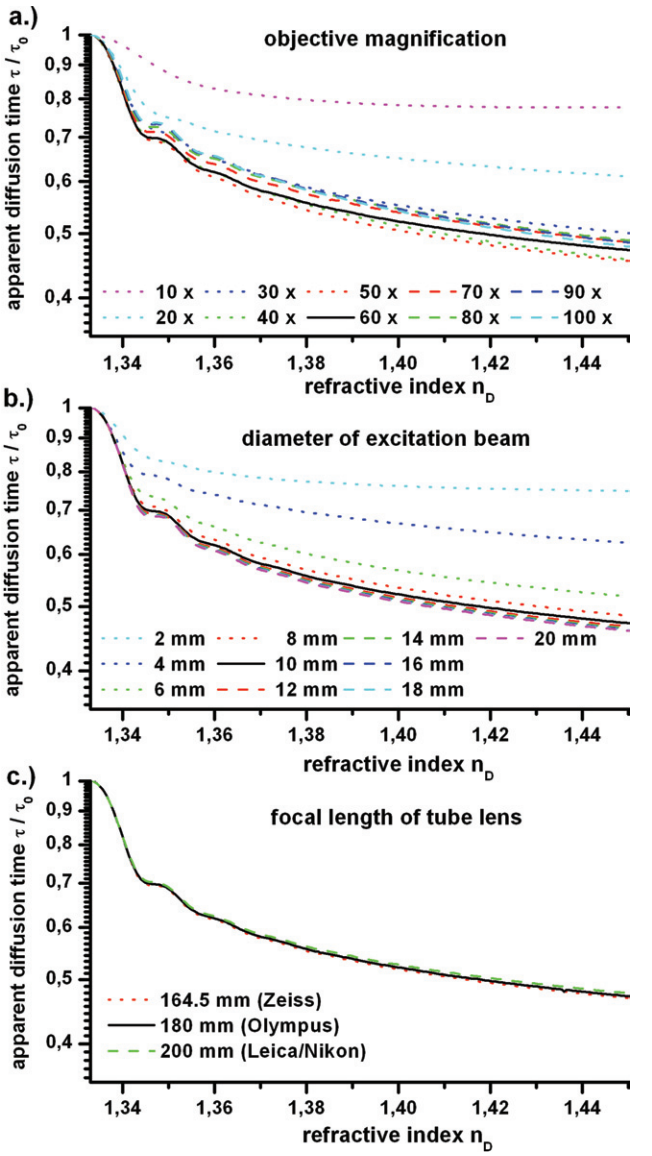

Fig. 3 Influence of instrumental design parameters [(a) objective magnification, (b) diameter of excitation beam, (c) focal distance of tube lens] due to the refractive index dependency of the apparent diffusion time. Simulation parameters if not indicated: focus position = 100 μm, λ_{ex} = 530 nm, $\lambda_{em} = \lambda_{ex}$ + 40 nm, confocal aperture = 50 μm, objective magnification = 60×, excitation beam diameter = 10 mm and tube lens focal distance = 180 mm.

4.1.1 Experimental parameters. To calculate apparent diffusion times, displayed as straight black lines in Fig. 2 and 3, we consider the following parameter values: focus position = 100 μm, λ_{ex} = 530 nm, $\lambda_{em} = \lambda_{ex}$ + 40 nm, confocal aperture = 50 μm, objective magnification = 60×, excitation beam diameter = 10 mm and tube lens focal distance = 180 mm.

The focus position in the sample was measured from the sample side of the cover slip surface, by moving the objective towards the sample by the indicated distance. Please note that the actual focus position is farther away from the cover slip surface than what would be expected from the positioning of the objective. The additional displacement, due to refractive index mismatch, is not obviously visible for the experimenter. Therefore we indicate the shift of the objective.

The maximum possible distance of the focus from the cover slip surface depends on the objective magnification and is on the order of 200 μm. Larger objective magnification decreases this range, therefore 100 μm was selected as the standard parameter for our calculations.

The excitation wavelength was chosen to be in the middle of the visible spectra, λ_{ex} = 530 nm and the emission wavelength was set to λ_{em} = 570 nm. For conventional single-focus FCS on a MT200 setup, a confocal aperture with a typical diameter of

50 μm is used as standard parameter for simulations. In all plots, dashed lines indicate parameter values larger and dotted lines values smaller that those of the reference indicated by the straight black line.

In Fig. 2a, the focus position was varied between 10 μm and 200 μm which is the typical range for FCS experiments. As can be seen in the plot, this parameter has the strongest influence on the apparent diffusion times. Unfortunately, this parameter is the value which is most easily misaligned by the experimenter during sample change. Therefore, positioning the sample with an accuracy better than ±1 μm is strongly recommended, as described, for example, in ref. 24.

Fig. 2b shows the wavelength dependency. We consider a constant Stokes shift of 40 nm between excitation and emission wavelength. The examined range covers the whole visible range, so our results are applicable for nearly all fluorescent dyes. The type of fluorescent dye is typically not changed during a series of experiments, but for optimizing experimental conditions, it is noted that dyes with longer excitation wavelengths lead to smaller refractive index dependencies of apparent diffusion time.

Fig. 2c presents results for the diameter of the confocal aperture, varied between 25 μm and 200 μm. In a number of commercial FCS instruments, the diameter of the confocal aperture can be tuned by the experimenter. Sometimes this parameter is used to increase the sensitivity of the instrument, because a bigger aperture allows for the passage of more photons. We assume that the confocal aperture is not changed *during* one series of crowding experiments. In what follows, we consider only the general influence of the confocal aperture diameter. This parameter has a strong influence on the size and volume of the confocal detection region. Smaller apertures lead to a smaller detection volume, which is typically desired in FCS experiments. Remarkably, a smaller confocal aperture decreases the refractive index dependent effects in the measurements.

4.1.2 Instrumental parameters. In this section, we focus on the design parameters of a conventional FCS instruments.

In Fig. 3a the influence of different objective magnifications is presented. As can be seen, the difference between objectives with a magnification larger than 30× has only minor influence, because at this magnification one already operates at the diffraction limit. In general, higher objective magnifications lead to smaller confocal volumes, as usually desired in confocal experiments, but application of objective magnifications larger than 60× are not leading to better results, due to the diffraction limit.

The influence of the excitation beam diameter is shown in Fig. 3b, investigated over a range from 2 mm to 20 mm. Smaller excitation beam diameters lead to imperfect focusing. As presented in the plot, the diffraction limit is reached for a beam diameter larger than 12 mm. The excitation beam diameter has a direct influence on the MDF size. Smaller excitation beam diameters lead to bigger MDF sizes. This parameter is used to make the experiment less sensitive for deviations caused by refractive index mismatch, but at the cost of a small detection volume.

The last evaluated parameter is the focal length of the tube lens. Most commercial systems use setups with a microscope from one of the manufactures Zeiss (focal length 164.5 mm), Olympus (focal length 180 mm), Leica or Nikon (focal length 200 mm). As can be seen in Fig. 3c, the focal distance of the tube lens has nearly no influence on the artifacts induced by refractive index mismatch. Therefore, this parameter provides no margin to improve the system performance.

4.2 Molecular crowding of dextrane in dextrane system

Dextranes are often used as crowding agents as well as tracers to investigate local viscosity in biological systems due to the biocompatibility of these molecules. Typically, the unlabeled dextrane is used as crowding agent and FITC labeled dextrane as the tracer molecule. The same size of crowding agent and tracer molecule enables the investigation of the self-diffusion of the dextranes.

To characterize crowding, refractive index and viscosity were studied as shown in Fig. 4 *a*. The refractive index shows a linear

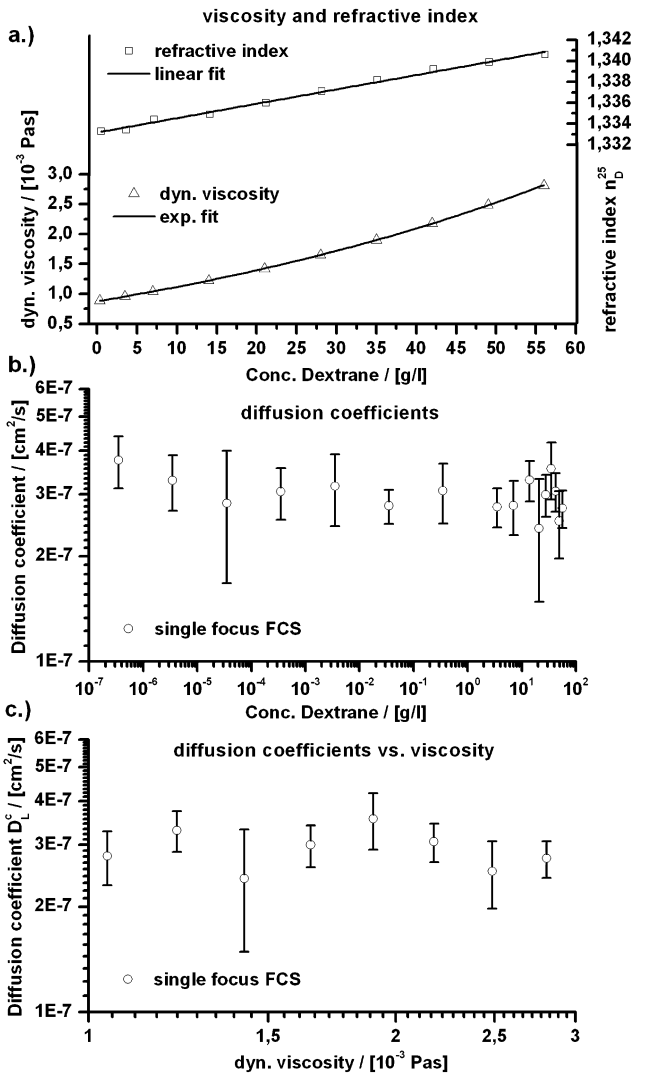

Fig. 4 Molecular crowing in 70 kDa dextrane–dextrane system. (a) Refractive index and dynamic viscosity. (b) Single-focus FCS data evaluation with out any further correction. Diffusion coefficients are referenced against Rhodamine 6G diffusion coefficient 2.80 × 10^6 cm^2/s in water at 25.0 °C, as used in most publications. (c) Self diffusion coefficient $D_L{}^c$ obtained from single-focus FCS data evaluation, *versus* dynamic viscosity η of 70 kDa FITC dextrane–dextrane system. For the experiments, a water immersion objective, which is corrected for immersion liquid with $n_D = 1.333$, is used.

behavior over the studied concentration range, where the refractive index for the highest concentration ($c = 56$ g/l) was determined as $n_D^{25.0\,^{\circ}C} = 1.341$. The viscosity shows an exponential behavior with a dynamic viscosity of $\eta_{25.0\,^{\circ}C} = 2.812 \times 10^{-3}$ Pas at a concentration of $c = 56$ g/l.

To study the self-diffusion in a crowded environment we performed 2fFCS experiments. We evaluated also the ACFs with a single-focus FCS data evaluation where we used the two ACFs from the two foci of the 2fFCS measurements as two simultaneous single-focus FCS experiments.

FCS probes the diffusion on a length scale that is much longer as compared to the size of the crowding agent and the correlation length of the solution. Therefore we assume that one has a linear relation between mean-square displacement of a particle and time. In principle, by repeating the same 2fFCS measurement with different interfocal distances, it could be possible to discern deviations form that behaviour, which would manifest itself in measuring different diffusion coefficients for different interfocal distances. However, this goes far beyond the scope of the present paper.

4.2.1 Single-focus FCS evaluation. Single-focus FCS evaluation is prone to a large number of possible artifacts, especially those induced by refractive index mismatch. In single-focus FCS measurements, the shape parameter of the MDF and the effective detection volume V_{eff} have to be determined by calibration measurements. Typically, this calibration is performed at the beginning of the experiments. For conventional FCS experiments, the length to diameter ratio κ of the MDF has to be determined by a z-scanning of a point-like fluorescence emitter. This is normally done with fluorescent latex particles with diameter of approx. 100 nm, immobilized on the surface of a cover glass. As shown in the preceding theoretical section, this leads to the first problem, because κ depends strongly on the refractive index as shown in Fig. 1.

Next, V_{eff} has to be determined by measuring a known diffusion standard like Rhodamine 6G and adjusting the value for V_{eff} to fit the calculated diffusion coefficient to that of the reference. As pointed out in ref. 44, the diffusion coefficient of Rhodamine 6G is $D_{\mathrm{Rh}}^{25.0\,^{\circ}C} = 4.14 \pm 0.05 \times 10^{-6}$ cm^2/s which differs from the often used value $D_{\mathrm{Rh}}^{25.0\,^{\circ}C} = 2.80 \pm 0.7 \times 10^{-6}$ cm^2/s. To be comparable with the "standard procedure" of FCS data evaluation, we used the "old" value for Rhodamine 6G of $D_{\mathrm{Rh}}^{25.0\,^{\circ}C} = 2.80 \times 10^{-6}$ cm^2/s as published in ref. 43.

To calculate the values of diffusion coefficients, as presented in Fig. 4b, the "conventional" diffusion model presented in ref. 40–43 for single species diffusion without triplet state dynamics is used. Each concentration was measured five times with the 2fFCS setup, leading to ten ACFs. The indicated error bars are the standard deviations of the ten ACFs per concentration. As can be seen, the error bars show deviations, that are larger than those expected from only the presence of a crowded environment. The comparison between the diffusion coefficient and the viscosity, as presented in Fig. 4b, cannot be further evaluated, because the data do not show any systematic trend, when taking into account the large error bars.

4.2.2 2fFCS evaluation. The same 2fFCS dataset is evaluated with the 2fFCS model. Typical correlation functions and the fitted model, eqn 6, are presented in Fig. 5a. 2fFCS enables measurement from concentrations close to the limit of infinite dilution (to determine the hydrodynamic radii (R_{h}) where intermolecular interaction of molecules can be neglected), up to concentrations where molecular interaction is observed, namely over a concentration range of eight orders of magnitude. It is interesting to notice, that the standard deviation, as derived from five ACF-pairs, is much smaller than that shown in Fig. 4b.

At lowest sample concentration ($c = 3.5 \times 10^{-7}$ g/l), 2fFCS yields diffusion coefficients for the 70 kDa FITC-dextranes of $D_{25.0\,^{\circ}C} = 3.31 \pm 0.21 \times 10^{-7}$ cm^2/s corresponding to $R_h = 7.4 \pm 0.5$ nm.

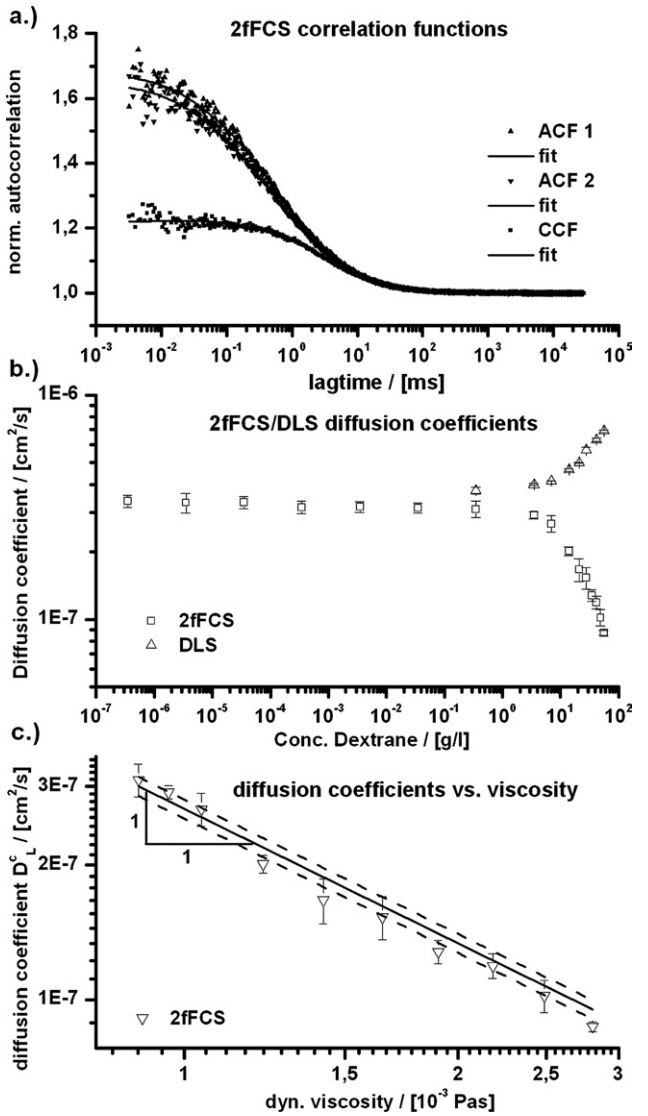

Fig. 5 Molecular crowing in 70 kDa dextrane–dextrane system. (a) Typical 2fFCS measurement of 70 kDa FITC-dextrane, correlation functions evaluated with eqn 6. (b) Comparison of 2fFCS and DLS results shows good agreement on low sample concentrations between both methods. (c) Self diffusion coefficient $D_L{}^c$ *versus* dynamic viscosity η of 70 kDa FITC dextrane–dextrane system. Dotted lines indicates 2fFCS accuracy of ±5%. For the experiments, a water immersion objective, which is corrected for immersion liquid with $n_D = 1.333$, is used. Please notice the different scales of the plots in Fig. 4 and Fig. 5.

This is in good agreement with literature[45] and with the results observed by Arrio-Dupont *et al.*,[46] where FITC dextrane with average molecular weight of 71.2 kDa was investigated by fluorescence recovery after photo bleaching (FRAP). There, the diffusion coefficient for 71.2 kDa FITC-dextrane was determined to be $D_{25.0\ ^\circ C} = 3.0 \pm 0.2 \times 10^{-7}$ cm²/s corresponding to a $R_h = 7.15 \pm 0.5$ nm.

The overlap concentration is estimated according to eqn 8

$$c^* = \frac{3M}{4\pi R_h^3 N_A} \tag{8}$$

and determined to be ($c^* \approx 60 \pm 10$ g/l). For sample concentrations close to the overlap concentration c^*, 2fFCS shows a decrease and DLS an increase of the diffusion coefficient. DLS integrates concentration fluctuations over a large molecule ensemble. The resulting diffusion coefficient at larger sample concentrations is therefore related to the short-time collective diffusion coefficient D_s^c. Due to the low scattering intensity, it is not possible to measure the diffusion coefficient of samples with $c < 0.35$ g/l by means of DLS. The interaction between dextrane molecules becomes more pronounced with increasing concentration, leading to an increase of the collective diffusion coefficient D_s^c, and a slow-down of tracer diffusion D_L^c as measured by 2fFCS.

In Fig. 5c , the evaluation of the self diffusion coefficient D_L^c *versus* dynamic viscosity η is presented. For a double logarithmic scaling, the relation between D_L^c and η is linear. As expected from eqn 7, the data agree well with a linear relationship of slope $= -1$.

In recent publications, Verkman and co-workers have demonstrated that a system does not show anomalous diffusion behavior if crowding agent and tracer have similar size.[13,47] Verkman studied various systems, containing labeled dextranes, DNA, albumin and nanospheres as tracer, and Ficoll 70, glycerol, albumin, and dextranes as crowding agents. Our data also reveal that crowding slows down the diffusion of solutes in aqueous phase compartments without leading to anomalous diffusion. The diffusion of the tracer depends only on the macroscopic viscosity, without any anomalous diffusion contribution. In contrast to published results by Verkman and co-workers, the 2fFCS technique allows studying the transition region more precisely. The presented data by Dauty and Verkman[13] comprises crowding agent concentrations from 0 wt% to 20 wt% and we have studied concentrations from 0 wt% to 5.5 wt% in small increments. The diffusion coefficient of the tracer is slowed down by the crowding agent, however the calculated tracer diffusion coefficient is also influenced by the refractive index mismatch as shown in Fig. 2 and Fig. 3. As can be seen from theoretical calculations in Fig. 2 and Fig. 3 the impact of refractive index mismatch has a non dependence on the refractive index and therefore on the concentration of the crowding agent. This leads to the conclusion, that conventional single FCS experiments show the effect of molecular crowding in experiments with a wide concentration range of crowding agent, where the measured diffusion coefficient is mainly dominated by the crowding agent. The systematic measurement error, the effect of refractive index mismatch, is within the accuracy of the single focus FCS technique. The 2fFCS technique is robust against systematic error of refractive index mismatch and offers the possibility of studying crowding also in the transition region between unhindered and hindered diffusion, where the effect of refractive index mismatch is dominating the measured diffusion coefficient.

5 Conclusions

For highly accurate diffusion measurements over the transition region from free to hindered diffusion, conventional FCS reaches its limits, yielding incorrect values for the measured diffusion coefficient. This is mostly due to the refractive index mismatch between the refractive indices of the sample and the refractive index of the immersion liquid. In contrast to standard single focus FCS experiments, the novel technique of 2fFCS provides a much higher accuracy of measured diffusion coefficients and is additionally robust against detrimental effects of refractive index mismatch.

We presented wave-optical calculations of the molecule detection function, which are then used to investigate the influence of various experimental parameters on the outcome of FCS measurements. The studied parameters have been: focus position, wavelength and confocal aperture size, objective magnification, excitation beam diameter, and focal distance of tube lens.

2fFCS is rather immune to the manifold problems of conventional FCS and is capable of absolutely measuring diffusion coefficients in samples with refractive index mismatch without further calibration. This is demonstrated by studying the transition range of a 70 kDa dextrane–dextrane system as an example for self-diffusion of dextranes in a crowded environment. 2fFCS results are compared with short time collective diffusion coefficients gained by DLS experiments. For diluted samples, 2fFCS and DLS show equal results, but 2fFCS is capable to measure at seven orders of magnitude lower concentrations than DLS. The comparison of the diffusion coefficient obtained by 2fFCS versus experimental values from viscosity measurement, shows a linear dependency with a slope $= -1$ according to the Stokes–Einstein equation. For our 70 kDa dextrane–dextrane system, where the tracer and the crowding agent have similar size, we expect non-anomalous diffusion behavior as demonstrated by Verkman and co-workers.[13,47]

The results demonstrate that 2fFCS is an excellent tool to probe quantitatively the diffusion of tracer molecules in complex fluids and is also able to study the transition from free- to hindered diffusion in crowded systems.

Acknowledgments

We are indebted to PicoQuant Company (Berlin, Germany) for their technical support. Financial support by the Deutsche Forschungsgemeinschaft (SPP1259) is gratefully acknowledged.

References

1 H. Zettl, U. Zettl, G. Krausch, J. Enderlein and M. Ballauff, *Physical Review E (Statistical, Nonlinear, and Soft Matter Physics)*, 2007, **75**(6), 061804–6.
2 T. Bonné, C. Papadakis, K. Lüdtke and R. Jordan, *Colloid Polymer Science*, 2007, **285**(5), 491–497.
3 J. Szymanski, A. Patkowski, A. Wilk, P. Garstecki and R. Holyst, *J. Phys. Chem. B*, 2006, **110**(51), 25593–25597.
4 O. Seksek and A. S. Verkman, *Biophysical Journal*, 1997, **72**(2), Tu372–Tu372.

5 S. B. Zimmerman and A. P. Minton, *Annual Review of Biophysics and Biomolecular Structure*, 1993, **22**(1), 27–65.
6 A. P. Minton, *J. Biol. Chem.*, 2001, **276**(14), 10577–10580.
7 R. M. Macnab, *Science*, 2000, **290**(5499), 2086–2087.
8 S. Asakura and F. Oosawa, *Journal of Polymer Science*, 1958, **33**(126), 183–192.
9 S. Zorrilla, M. A. Hink, A. J. Visser and M. P. Lillo, *Biophysical Chemistry*, 2007, **125**(2–3), 298–305.
10 D. S. Banks and C. Fradin, *Biophys. Journal*, 2005, **89**(5), 2960–2971.
11 H. Neuweiler, M. Löllmann, S. Doose and M. Sauer, *Journal of Molecular Biology*, 2007, **365**(3), 856–869.
12 D. J. Winzora and P. R. Wills, *Biophysical Chemistry*, 2006, **119**(2), 186–195.
13 E. Dauty and A. S. Verkman, *Journal of Molecular Recognition*, 2004, **17**(5), 441–447.
14 H. Sanabria, Y. Kubota and M. N. Waxham, *Biophys. J.*, 2007, **92**(1), 313–322.
15 A. Michelman-Ribeiro, F. Horkay, R. Nossal and H. Boukari, *Biomacromolecules*, 2007, **8**(5), 1595–1600.
16 S. T. Hess and W. W. Webb, *Biophysical Journal*, 2002, **83**(4), 2300–2317.
17 T. Dertinger, A. Loman, B. Ewers, C. B. Müller, B. Krämer and J. Enderlein, *Opt. Express*, 2008, **16**(19), 14353–14368.
18 T. Dertinger, V. Pacheco, I. von der Hocht, R. Hartmann, I. Gregor and J. Enderlein, *ChemPhysChem*, 2007, **8**(3), 433–443.
19 J. Enderlein, I. Gregor, D. Patra, T. Dertinger and B. Kaupp, *ChemPhysChem*, 2005, **6**(11), 2324–2336.
20 J. Enderlein, I. Gregor, D. Patra and J. Fitter, *Current Pharmaceutical Biotechnology*, 2004, **5**(2), 155–161.
21 C. B. Müller, K. Weiß, W. Richtering, A. Loman and J. Enderlein, *Opt. Express*, 2008, **16**(6), 4322–4329.
22 C. B. Müller, A. Loman, W. Richtering and J. Enderlein, *J. Phys. Chem. B*, 2008, **112**(28), 8236–8240.
23 C. B. Müller, K. Weiß, A. Loman, J. Enderlein and W. Richtering, *Lab on a Chip*, 2008, DOI: 10.1039/b807910b.
24 C. B. Müller and W. Richtering, *Colloid & Polymer Science*, 2008, **286**(11), 1215–1222.
25 E. Wolf, *Proceedings of the Royal Society of London. Series A, Mathematical and Physical Sciences (1934–1990)*, 1959, **253**(1274), 349–357.
26 B. Richards and E. Wolf, *Proceedings of the Royal Society of London. Series A, Mathematical and Physical Sciences (1934–1990)*, 1959, **253**(1274), 358–379.
27 P. Török and P. Varga, *Applied Optics*, 1997, **36**(11), 2305–2312.
28 P. Török, P. Varga, Z. Laczik and G. Booker, *J. Opt. Soc. Am. A*, 1995, **12**(2), 325–332.
29 O. Haeberlé, *Optics Communications*, 2004, **235**(1–3), 1–10.
30 A. Egner, M. Schrader and S. W. Hell, *Optics Communications*, 1998, **153**(4–6), 211–217.
31 O. Haeberlé, M. Ammar, H. Furukawa, K. Tenjimbayashi and P. Török, *Opt. Express*, 2003, **11**(22), 2964–2969.
32 I. Gregor and J. Enderlein, *Opt. Lett.*, 2005, **30**(19), 2527–2529.
33 M. Leutenegger, R. Rao, R. Leitgeb and T. Lasser, *Opt. Express*, 2006, **14**(23), 11277–11291.
34 L. Allen and M. J. Padgett, *Optics Communications*, 2000, **184**(1–4), 67–71.
35 P. Török, P. D. Higdon and T. Wilson, *Journal of Modern Optics*, 1998, **45**, 1681–1698.
36 P. D. Higdon, P. Török and T. Wilson, *Journal of Microscopy*, 1999, **193**, 127–141.
37 P. Török, *Opt. Lett.*, 2000, **25**(19), 1463–1465.
38 M. Leutenegger and T. Lasser, *Opt. Express*, 2008, **16**(12), 8519–8531.
39 A. Loman, T. Dertinger, F. Koberling and J. Enderlein, *Chem. Phys. Lett.*, 2008, **459**, 18–21.
40 M. Ehrenberg and R. Rigler, *Chemical Physics*, 1974, **4**(3), 390–401.
41 D. Magde, W. W. Webb and E. Elson, *Physical Review Letters*, 1972, **29**(11), 705–708.
42 E. L. Elson and D. Magde, *Biopolymers*, 1974, **13**(1), 1–27.
43 D. Magde, E. L. Elson and W. W. Webb, *Biopolymers*, 1974, **13**(1), 29–61.
44 C. B. Müller, A. Loman, V. Pacheco, F. Koberling, D. Willbold, W. Richtering and J. Enderlein, *Europhysics Letters*, 2008, **83**(4), 46001.
45 J. Brandrup, E. H. Immergut and E. A. Grulke, *Polymer Handbook*, Wiley-Interscience, New York, fourth edn, 1999.
46 M. Arrio-Dupont, S. Cribier, G. Foucault, P. F. Devaux and A. d'Albis, *Biophys. J.*, 1996, **70**(5), 2327–2332.
47 J. A. Dix and A. S. Verkman, *Annual Review of Biophysics*, 2008, **37**(1), 247.

